

## The Mass of the Black Hole in the X-ray Binary M33 X-7 and the Evolutionary Status of M33 X-7 and IC 10 X-1

M. K. Abubekero, E. A. Antokhina, A. I. Bogomazov, and A. M. Cherepashchuk

*Sternberg Astronomical Institute, Moscow State University,  
Universitetskii pr. 13, Moscow, 119899, Russia*

Received June 24, 2008; in final form, July 2, 2008

**Abstract**—We have analyzed the observed radial-velocity curve for the X-ray binary M33 X-7 in a Roche model. We have analyzed the dependence between the component masses and the degree of filling of the optical star's Roche lobe to obtain the ratio of the masses of the optical star and compact object. For the most probable mass of the optical star,  $m_v = 70 M_\odot$ , the mass of the compact object is  $m_x = 15.55 \pm 3.20 M_\odot$ . It has been shown that black holes with masses of  $m_x = 15 M_\odot$  and even higher can form in binaries. We present characteristic evolutionary tracks for binary systems passing through an evolutionary stage with properties similar to M33 X-7-type objects. According to population-synthesis analyses, such binaries should be present in galaxies with masses of at least  $10^{11} M_\odot$ . The present number of such systems in M33 should be of the order of unity. We have also studied the evolutionary status of the X-ray binary IC 10 X-1 with a Wolf–Rayet component, which may contain a massive black hole. The final stages of the evolution of the M33 X-7 and IC 10 X-1 systems should be accompanied by the radiation of gravitational waves.

PACS numbers: 97.80.Jp, 97.80.Fk, 97.10.Nf, 97.10.Cv, 97.60.Lf

DOI: 10.1134/S1063772909030056

### 1. INTRODUCTION

The X-ray source M33 X-7 (which we will call X-7) is situated in the galaxy M33 X-7 [1]. The periodic variability of the source was first detected by Peres et al. [2, 3], whose gave the first estimate for the variability period  $P_{orb} = 1.7857^d$  and suggested that the X-ray source was in a stellar binary system.

Based on X-ray data obtained by the Einstein Observatory, ROSAT, and ASCA, Larson and Schulman [4] refined the period of the X-ray variability in the binary,  $P_{orb} = 3.4531^d$ . This value was confirmed by Dubus et al. [5]:  $P_{orb} = 3.4535^d \pm 0.0005^d$ .

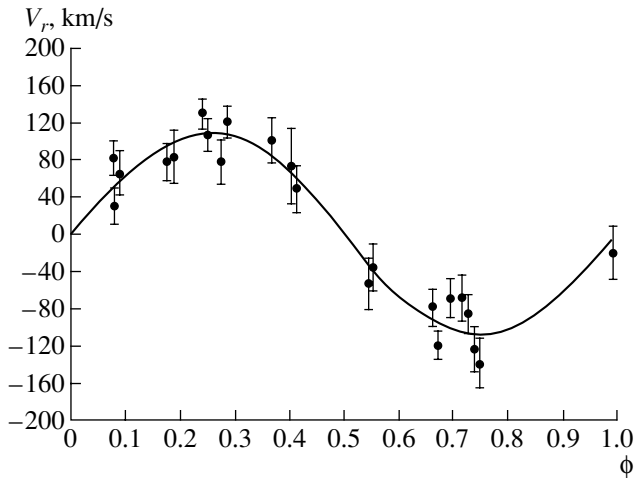
In 2004, the X-ray source X-7 was identified with an optical star of magnitude 18.89<sup>m</sup> [7]. Photometric observations in *B* and *V* [7] confirmed that X-7 was in a binary, and showed that the spectral type of the optical component of X-7 is B0I–O7I and its mass is  $m_v = 25–35 M_\odot$  [7]. The refined period of the binary (based on XMM-Newton and Chandra X-ray data)  $P_{orb} = 3.45376^d \pm 0.00021^d$  was obtained [7].

Based on the Einstein, ROSAT, and XMM-Newton data, Pietsch et al. [6] derived the new period  $P_{orb} = 3.453014^d \pm 0.000020^d$ . HST observations of the OB association HS 13, which contains X-7, yielded the refined spectral type for the optical component O6 III, and a minimum mass of  $m_v = 20 M_\odot$  [6].

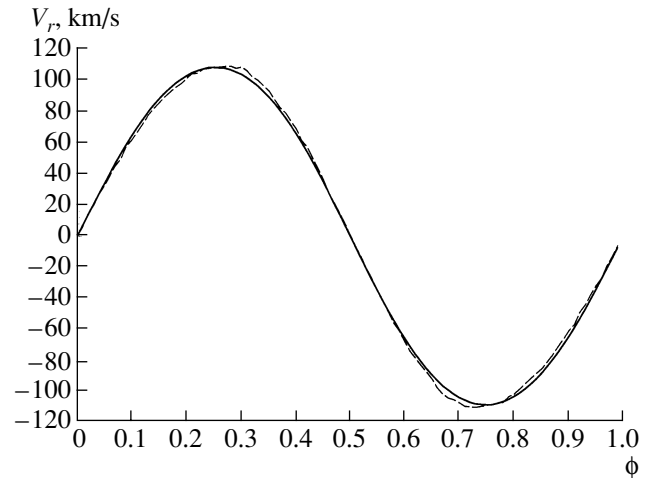
Based on the spectral type of the optical component, the rate of variation of the binary period, the absence of an X-ray pulsar, and the analysis of the X-ray spectrum and optical light curves of [7], Pietsch et al. [6] suggested that X-7 is a black hole (BH).

A detailed analysis of the photometric light curves of X-7 is presented in [8]. The photometric period of the binary was  $P_{orb} = 3.4530^d \pm 0.0014^d$ . The radius of the optical component is  $R = 15–20 R_\odot$ , and its effective temperature  $T_{eff} = 33\,000–47\,000$  K [8].

The first dynamical estimate of the mass of the compact object in X-7 was derived from the observed radial-velocity curve in [9]:  $m_x = 15.65 \pm 1.45 M_\odot$ . The average mass for most black-hole candidates in close binary systems is near  $m_x \sim 8 M_\odot$ . The mass of the compact object in X-7 significantly exceeds this estimate. Note that the mass of the compact object was estimated for a point-mass model in [9]. In addition, the errors of the observed radial-velocity curve are large (about 20%–30% of the half-amplitude), which certainly affects the accuracy of the estimated mass of the compact object. Having in mind the importance of a reliable mass for the compact object in X-7 for our understanding of the evolution of binary stars, we have analyzed the observational data of [9] in a Roche model [10, 11]. We have also analyzed the



**Fig. 1.** Observed and theoretical radial-velocity curve for the optical component in the X-ray binary M33 X-7. The points show the radial velocities of the optical star taken from [9]. The solid curve shows the theoretical radial-velocity curve in the Roche model calculated for a mass of the compact object  $m_x = 15.55 M_\odot$ , a mass of the optical star  $m_v = 70 M_\odot$ , and the orbital inclination  $i = 74.6^\circ$  (the remaining parameters of the binary are presented in Table 1).



**Fig. 2.** Theoretical radial-velocity curves for the optical star, obtained in the Roche model with the mass of the compact object  $m_x = 15.55 M_\odot$ , the mass of the optical star  $m_v = 70 M_\odot$ , and the orbital inclination  $i = 74.6^\circ$  (the other parameters of the binary are presented in Table 1). The solid and dashed curves represent the radial-velocity curves calculated from the  $H\gamma$  and HeII 4200 Å absorption lines, respectively.

evolutionary status of the X-7 system and the evolution of the X-ray binary IC 10 X-1, which contains a Wolf–Rayet (WR) star and a possible black hole with a mass of  $m_x \sim 23 M_\odot$ .

## 2. OBSERVATIONAL DATA

We used the spectral data of [9] obtained from August 18 to November 16, 2006 on the 8.2-m Gemini North Telescope at wavelengths  $\lambda = 4000\text{--}5000 \text{ \AA}$ . The radial-velocity curve was derived from 22 spectra using the cross-correlation method together with a synthetic spectrum for  $\lambda = 4150\text{--}4300 \text{ \AA}$  and  $\lambda = 4521\text{--}4578 \text{ \AA}$ . These wavelength intervals contain the HeII 4200 Å and HeII 4541 Å lines, unblended by nebular lines. Orosz et al. [9] used the time for the middle of the X-ray eclipse of X-7 as the zero phase,  $T_0(\text{HJD}) = 2453967.157 \pm 0.048$  (this is fully consistent with the zero phase obtained previously in [6], and differs from it by  $95.001 \pm 0.014$  orbital cycles). The binary orbital period  $P_{orb} = 3.453014^d$  [9] was obtained from the X-ray light curve. Figure 1 presents the observed radial-velocity curve.

Since the data of [9] are not presented in numerical form, we digitized their observed radial-velocity curve with an accuracy for the radial velocity of the optical component  $\sim 0.6 \text{ km/s}$ , which is substantially smaller than the mean error of the observed radial velocities,

$\sim 20\text{--}25 \text{ km/s}$ . Therefore, the accuracy of our digitization of the observed radial-velocity curve from [9] is fully suitable for our further analysis.

## 3. ANALYSIS FOR THE OBSERVED RADIAL-VELOCITY CURVE

The distance between the components in the X-7 binary system is comparable to the radius of the optical star. The degree of Roche-lobe filling by the optical component in X-7 is  $\mu = 0.777 \pm 0.017$  [9]. The point-mass model used to interpret the radial-velocity curve in [9] does not allow taking into account the proximity of the components.

In this connection, we analyzed the radial-velocity curve for the optical component of X-7 in a Roche model, which enables us in a first approximation to take into account the tidal deformation of the star and the non-uniform temperature distribution over its surface, due to the effects of gravitation darkening and heating of the star's surface by X-rays from the relativistic object. The effect of X-ray heating in this system is insignificant. The bolometric luminosity of the optical component for the adopted effective surface temperature  $T_{eff} = 35\,000 \text{ K}$  is  $L_v = 1.3 \times 10^{39} \text{ erg/s}$ . The average luminosity of the X-ray source out of eclipse is  $L_x = 5 \times 10^{37} \text{ erg/s}$  [6]. Thus,  $k_x = L_x/L_v \simeq 0.04$  (in spite of the small amount of X-ray heating of the surface of the optical star,

**Table 1.** Parameters used in modeling the radial-velocity curves for the optical component in the Roche model

$P$ , days	3.453014	Orbital period
$m_v$ , $M_\odot$	varied*	Mass of the optical star
$e$	0.0	Eccentricity
$i$	$74.6^\circ$	Orbital inclination
$\mu$	0.78–1.0**	Roche-lobe filling factor for the optical component
$f$	1.0	Asynchronicity factor for the rotation of the optical component
$T_{eff}$ , K	35 000	Average effective temperature of the optical component
$\beta$	0.25	Gravitational darkening coefficient
$k_x$	0.04	Ratio of the X-ray luminosity of the relativistic component to the bolometric luminosity of the optical component $L_x/L_v$
$A$	1.0	Coefficient for reprocessing of the X-ray radiation
$x; y$	−0.186; −0.683	Limb darkening coefficient

\* The mass of the optical star was varied in the model calculations.

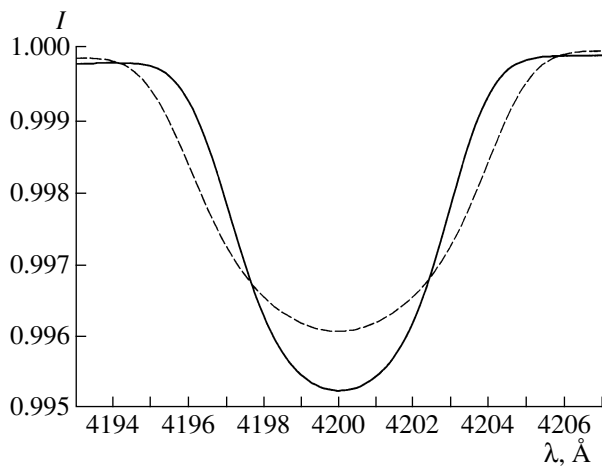
\*\*  $\mu$  was taken to be 0.78, 0.85, 0.90, 0.95, 1.0.

we including this heating when modeling the radial-velocity curve). Therefore, the radial-velocity curve for the optical component is mainly perturbed by tidal–rotational deformation of the star and gravitational darkening of its surface. The procedure used to model the radial-velocity curve is described in de-

tail by Antokhina and Cherepashchuk [10] and Antokhina [11]. Here, we briefly review the main elements of the method.

The binary system consists of the optical star, described by the Roche model, and a point-like X-ray source. The tidally deformed surface of the star was subdivided into  $\sim 2600$  surface elements, for each of which the emergent radiation was calculated, taking into account gravitation darkening, the heating of the star’s surface by radiation from its companion (the reflection effect), and limb darkening. The effect of heating of the star’s atmosphere by X-ray radiation from the companion was included in the procedure [10, 11] by adding the emergent and incident fluxes (without taking into account radiation transfer in the star’s atmosphere). Since the effect of X-ray heating is very small in X-7, this approximation is quite acceptable.

A model radial-velocity curve was calculated based on the  $H\gamma$  absorption line profile. The profile and its equivalent width for each visible surface element with local temperature  $T_{loc}$  and local gravitational acceleration  $g_{loc}$  were calculated by interpolating values in Kurucz’s tables for Balmer lines [12]. The integrated line profile at a given orbital phase was calculated by summing over the visible surface of the star, taking into account the Doppler effect for the local profiles, previously normalized to the continuum for each surface element (see [10, 11] for more detail). The calculated integrated absorption profile was used to determine the radial-velocity of the star. The radial velocity at a given orbital phase was calculated from the average wavelength at residual



**Fig. 3.** Model integrated profiles for the HeII 4200 Å absorption line of the optical component in X-7 at orbital phase 0.0. The profiles were obtained in the Roche model with  $m_x = 15.55 M_\odot$ ,  $m_v = 70 M_\odot$ , and  $i = 74.6^\circ$ . The solid and dashed curves represent the absorption-line profiles obtained in the Roche model for degrees of filling of the Roche lobe  $\mu = 0.78$  and  $\mu = 1.0$ , respectively (the other parameters of the binary are presented in Table 1). Both model integrated profiles were convolved with a spectrograph response function with  $\text{FWHM} = 2 \text{ \AA}$ .

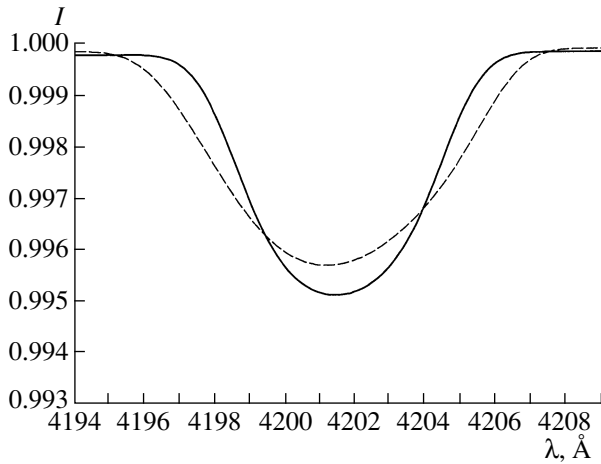


Fig. 4. Same as Fig. 3 for orbital phase 0.25.

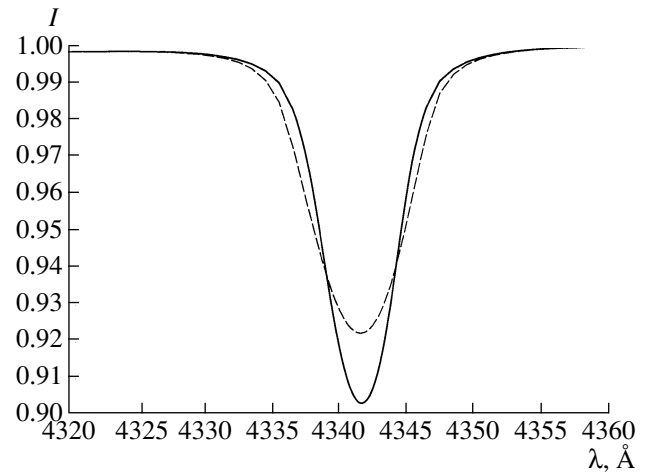


Fig. 5. Same as Fig. 4 for the H $\gamma$  absorption line.

intensity levels of 1/3, 1/2, and 2/3 of the depth of the integrated absorption profile. The limb darkening of the stellar disk was calculated using the square-root law  $I(\cos \theta) = I_0(1 - x(1 - \cos \theta) + y(1 - \sqrt{\cos \theta}))$ , where  $\theta$  is the angle between the direction towards the observer and the normal to the surface and  $x$  and  $y$  are the limb-darkening coefficients [13, 14].

Since the mass of the optical star is not known exactly, we treated the masses of both components of the binary as parameters of the model to be fit. We carried out an exhaustive search over the parameters and over multiple solutions for the fit. An exhaustive search for the mass of the compact object  $m_x$  was made for each mass of the optical component  $m_v$  from the discrete set of values 20, 30, 40, 50, 60, 70, and 80  $M_\odot$  and for the orbital inclination  $i = 74.6^\circ$ . The fit of the model to the observations was evaluated using the  $\chi^2$  criterion. We selected the significance level  $\alpha = 5\%$  (see [15] for more detail).

In [9], the observed radial velocities were obtained from fragments of spectra containing the HeII 4200 Å and HeII 4541 Å lines. Unfortunately, fitting the radial-velocity curve based on the HeII model line is very time-consuming. Therefore, as we indicated above, we constructed the theoretical radial-velocity curve using the model H $\gamma$  absorption line. Test calculations (Fig. 2) showed no qualitative difference between the model radial-velocity curves obtained from the HeII 4200 Å and H $\gamma$  lines; the average quantitative difference is 3–4 km/s, which is substantially smaller than the errors in the observed radial velocities,  $\Delta V_r \simeq 20\text{--}30$  km/s. The calculated radial-velocity curve derived for the HeII 4200 Å line was based on the model atmosphere for the optical star [16]. Figures 3–5 present model profiles of the HeII 4200 Å absorption line at the two orbital phases

$\phi = 0.0, 0.25$  and of the H $\gamma$  absorption line profile for Roche-lobe filling factors of  $\mu = 0.78$  and 1.0. The result of our analysis of the observed radial-velocity curve of [9] in the Roche model is presented in numerical form in Table 2 and graphically in Fig. 6.

Figure 7 presents the discrepancy  $\Delta$  between the observed and theoretical radial-velocity curves, whose minimum corresponds to the best-fit relationship between  $m_v$  and  $m_x$ . It is obvious that the Roche model for X-7 cannot be rejected at the  $\alpha = 0.05$  significance level. The model can be adopted, and

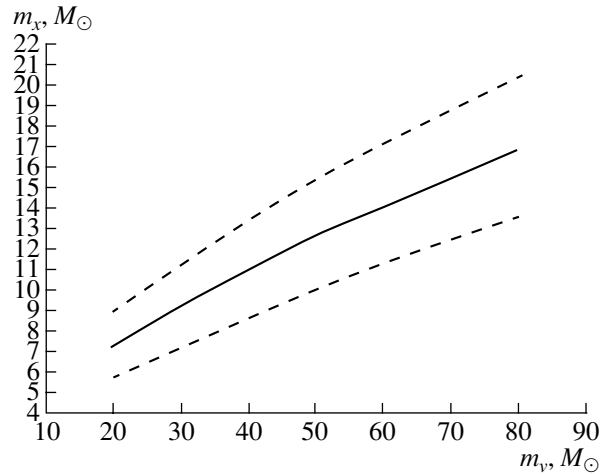


Fig. 6. Relationship between the masses of the compact object and optical component of X-7, obtained from the fit of the observed radial-velocity curve from [9] in the Roche model. The parameters of the binary are presented in Table 1. The solid curve represents the central values for the mass of the black hole, while the dashed curves correspond to the upper and lower boundaries for the errors on the central values based on the  $\chi^2_M$  statistics for the  $\gamma = 95\%$  confidence level ( $M$  is the number of observed points on the radial-velocity curve).

**Table 2.** Dependence of component masses in X-7 for  $i = 74.6^\circ$  (the errors correspond to the 95% confidence interval for  $\chi^2_M$  statistics, where  $M$  is the number of points in the radial-velocity curve)

$m_v, M_\odot$	$m_x, M_\odot$
20	$7.30 \pm 1.60$
30	$9.30 \pm 2.00$
40	$11.0 \pm 2.40$
50	$12.65 \pm 2.70$
60	$14.15 \pm 2.90$
70	$15.55 \pm 3.20$
80	$16.95 \pm 3.40$

**Table 3.** Difference between the half-amplitude of the radial-velocity curves obtained in the Roche and point-mass models,  $V_{Roche}$  and  $V_c$ , as a function of the degree of Roche-lobe filling by the optical star  $\mu$

$\mu$	$V_c - V_{Roche}, \text{km/s}$	$m_x, M_\odot^*$
0.78	0.80	15.55
0.85	1.43	15.60
0.90	2.11	15.65
0.95	3.24	15.75
1.00	6.11	15.95

\* Black-hole mass obtained in the Roche model for the mass of the optical star  $m_v = 70 M_\odot$ . The remaining model parameters are presented in Table 1.

the optimum values for the parameters and their confidence intervals (errors) at the  $\gamma = 1 - \alpha = 0.95$  confidence level can be estimated.

Our analysis using our more complex and physically more adequate model confirms the quantitative conclusions of [9]. Due to the small degree of Roche-lobe filling by the optical star, the black-hole masses obtained in our study and in [9] are quite similar:  $15.55 \pm 3.20 M_\odot$  and  $15.65 \pm 1.45 M_\odot$ , respectively (for the most probable mass of the optical star  $m_v = 70 M_\odot$ ).

Let us consider the dependence of the amplitude of the theoretical radial-velocity curve on the degree of Roche-lobe filling by the optical star. Figures 4 and 5 present the model HeII 4200 Å and H $\gamma$  absorption line profiles obtained for degrees of Roche-lobe filling by the optical star  $\mu = 0.78$  and 1.0. The “center of

gravity” for the absorption line obtained for  $\mu = 0.78$  is more shifted towards red wavelengths, compared to the position for complete filling of the Roche lobe; i.e., the half-amplitude of the radial-velocity curve of the optical star  $K_v$  decreases with increasing degree of Roche-lobe filling  $\mu$ .

The following calculations present the quantitative difference between the half-amplitude of the radial-velocity curves for the point-mass and Roche models for various degrees of Roche-lobe filling  $\mu$ . For these calculations, we took the masses of the compact and optical components to be  $m_x = 15.55 M_\odot$  and  $m_v = 70 M_\odot$ . The half-amplitude of the radial-velocity curve for these parameters of the binary was  $V_c = 108.65 \text{ km/s}$ . The difference of the half-amplitude of the radial-velocity curve presented in Table 3 is essentially independent of the orbital inclination of the binary (at least in the interval  $i = 60^\circ - 90^\circ$ ). It is obvious that the half-amplitude of the theoretical radial-velocity curve decreases with increasing  $\mu$ , and is 6.11 km/s smaller than the value for the point-mass model for  $\mu = 1.0$ . The mass of the relativistic object  $m_x$  in the Roche model increases with increasing  $\mu$ .

We can see from Table 3 that, up to  $\mu = 0.90$ , the difference between the half-amplitudes of the radial-velocity curves is close to  $\sim 1\%$  of the half-amplitudes themselves. When the Roche-lobe filling is even higher,  $\mu = 0.95 - 1.0$ , the half-amplitude of the radial-velocity curve decreases by  $\sim 3\% - 6\%$  compared to the half-amplitude for the point-mass model.

The results of fitting the observed radial-velocity curve for X-7 in the Roche model are close to those obtained for the point-mass model, even when the Roche lobe of the optical star is fully filled. For example, the difference between the mass of the compact object obtained in the Roche model for  $\mu = 0.78$  and in the point mass model is 0.6%, while this difference is 2.5% for  $\mu = 1.0$ . This closeness of the estimates for the mass of the compact object obtained in the Roche and point-mass models is not universal. For example, when a point-mass model is used to estimate the masses of X-ray pulsars in binaries with OB giants, the masses of the compact objects are systematically underestimated by up to  $\sim 10\%$  (see [17–19].) In the presence of substantial X-ray heating of the optical star, which appreciably changes the shape of the absorption profiles, the use of a point-mass model yields unrealistic results [20].

The similarity of the estimates for the mass of the compact object obtained in the Roche and point mass models for the binary X-7 is due to the fairly high mass of the compact object and the low degree of X-ray heating,  $k_x = 0.04$ . Thus, the fit of the observed

radial-velocity curve for the optical star in X-7 obtained for our more adequate model fully confirms the quantitative conclusions drawn in [9].

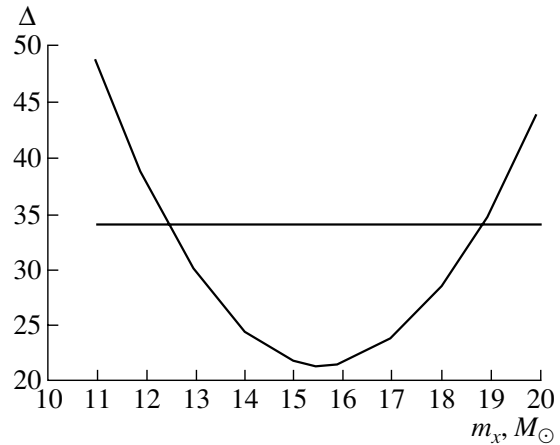
In spite of the fact that estimates of the mass of the optical component vary from 20 to 70  $M_{\odot}$ , we have adopted  $m_v = 70 M_{\odot}$  as the most probable value, since this is the value obtained from the most complete set of observational data: a spectral analysis, fitting of the light curve of the optical star, and the duration of the X-ray eclipse [9].

Based on the mass estimate  $m_v = 70 \pm 6.9 M_{\odot}$  [9], we find that the mass of the compact object is  $m_x = 14.5\text{--}16.5 M_{\odot}$ . As was already noted, this black-hole mass deviates substantially from the average value  $m_x \simeq 8 M_{\odot}$  for most binaries with black holes. We also emphasize the Roche model fit to the radial-velocity curve can be considered acceptable based on the  $\chi^2_M$  criterion at the  $\gamma = 95\%$  confidence level (where  $M$  is the number of observed points in the radial-velocity curve). Further, we consider evolutionary scenarios that can result in the formation of systems similar to X-7.

Recently [21], the minimum masses of the components of the binary IC 10 X-1, which consists of a Wolf–Rayet star and a compact object (proposed black hole) were estimated. The mass of the Wolf–Rayet star is  $m_v = 32.7 \pm 2.6 M_{\odot}$ , and the mass of the black hole obtained from the observed radial-velocity curve of the optical component is  $m_x = 23.1 \pm 2.1 M_{\odot}$ . Since no exact correspondence in time has been found between the eclipses of the components and the transition of the radial-velocity curve derived from the HeII 4200 Å emission line through the  $\gamma$  velocity, the conclusion that the black hole in this system has a high mass must be considered tentative. Nevertheless, we investigated the possible formation of a binary with these component masses.

#### 4. EVOLUTIONARY SCENARIOS FOR X-7 AND IC 10 X-1

The binary X-7 is considered from an evolutionary point of view in [9]. It was concluded that current evolutionary scenarios fail to explain the existence of systems similar to X-7. The problem encountered by some scenarios is as follows. Since the size of the initially more massive star exceeds the current distance between the components, the system should undergo a common-envelope stage, during which the components approach each other. However, for the formation of a black hole with a mass of about  $15 M_{\odot}$ , the star should fill its Roche lobe immediately after the completion of the helium burning in the core (followed by the common-envelope stage). The radius of the star should then be smaller than during core burning, and so the Roche lobe should not be filled.



**Fig. 7.** Dependence of the discrepancy  $\Delta$  between the observed and theoretical radial-velocity curve for  $m_v = 70 M_{\odot}$ . The horizontal line corresponds to the critical value for  $\chi^2$  at the  $\alpha = 0.05$  significance level.

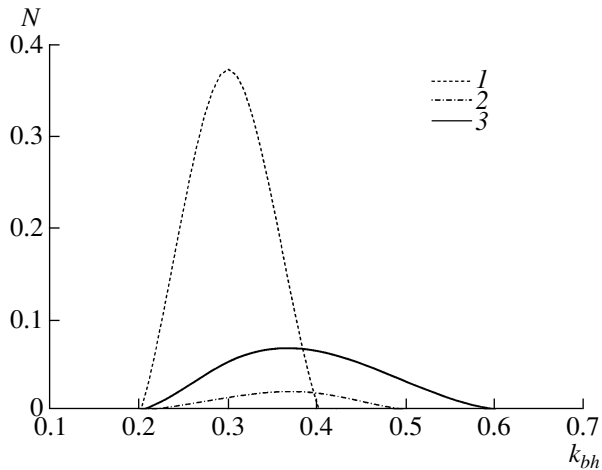
We analyzed possible evolutionary tracks for X-7 and IC 10 X-1 using the “Scenario Machine” code. The principles behind this code have been described repeatedly, and here we indicate only the basic parameters used in the calculations. A detailed description of the “Scenario Machine” can be found in [22, 23].

The mass functions for black holes in X-ray binaries were calculated for various evolutionary scenarios in [24]. One of the scenarios considered in [24] predicted the existence of black holes with masses up to  $50 M_{\odot}$ . This scenario satisfied the most important criterion for realistic evolutionary scenarios: the requirement that there exist Cyg X-1-type systems in the Galaxy.

A set of evolutionary scenarios A, B, C, and W are used in [24]<sup>1</sup>, which include various mass-loss rates, dependences of the core mass on the initial mass of the star, and “mass–radius” dependences. These scenarios are described in detail in [23, 24]. It was shown in [24] that scenario B must be rejected, since it cannot explain the existence of a Cyg X-1-type system in the Galaxy (that is not a statistical deviation). Therefore, we do not consider this evolutionary scenario here. Note that scenario B is based on the evolutionary assumptions presented in [9].

Let us consider the calculated evolutionary tracks for a binary system for evolutionary scenarios A, C,

<sup>1</sup> Note that scenarios A, B, C, and W represent various assumptions concerning the physical parameters of stars at various stages of their evolution, rather than specifications for types of mass exchange corresponding to the classification introduced by Kippenhahn and Weigert [25].



**Fig. 8.** Number of M33 X-7-type systems for a spiral galaxy with mass  $10^{11} M_{\odot}$  and a star-formation rate specified by the Salpeter function. The numbers indicate curves calculated for various sets of evolutionary parameters (see the text). The vertical axis plots the expected absolute number of M33 X-7-type systems in the Galaxy. The horizontal axis plots the fraction of the mass of the pre-supernova that is enclosed by the event horizon at the instant when the black hole is formed. In the case of curve “1” ( $\alpha = 0.3$ ,  $k_{WR} = 0.3$ ,  $k_{bh} = 0.3$ ), the maximum expected number of M33 X-7-type systems is 0.37, which is of the order of magnitude of unity.

and W. The latter two scenarios have a higher mass-loss rate than scenario A. In a first rough approximation, they can be taken to correspond to higher metallicities of the stars. The calculations indicate that X-7 or IC 10 X-1-type systems cannot be obtained from scenarios C and W. We have identified a domain of parameters in scenario A for which the formation of X-7 or IC 10 X-1-type systems appeared to be possible.

A more detailed description of evolutionary scenario A is given in [22–24], and here we only describe the parameters used as free parameters of the problem. In our modeling of possible binary precursors for X-7 and IC 10 X-1, the fraction and rate of mass loss in the main-sequence and Wolf–Rayet stages, as well as the fraction of the mass of the pre-supernova that was enclosed by the event horizon, were varied. The star’s mass-loss rate  $\dot{M}$  is very important for two reasons: it substantially affects both the semimajor axis of the binary and the mass of the star. The mass-loss rate  $\dot{M}$  in the main-sequence stage is described by the classical formula

$$\dot{M} = \frac{\alpha L}{cV_{\infty}}, \quad (1)$$

where  $L$  is the luminosity of the star,  $V_{\infty}$  the velocity of its wind at infinity,  $c$  the speed of light, and  $\alpha$  a free parameter. In scenario A, the change in the mass  $\Delta M$

during a single evolutionary stage does not exceed  $0.1(M - M_{core})$ , where  $M$  is the mass of the star at the beginning of the stage and  $M_{core}$  is the mass of the stellar core. We parametrized the mass loss at the Wolf–Rayet stage as  $\Delta M_{WR} = k_{WR}M_{WR}$ , where  $M_{WR}$  is the maximum mass of the star at this stage.

The mass of the black hole  $M_{BH}$  formed as a result of the explosion of a pre-supernova with mass  $M_{preSN}$  was calculated from the formula

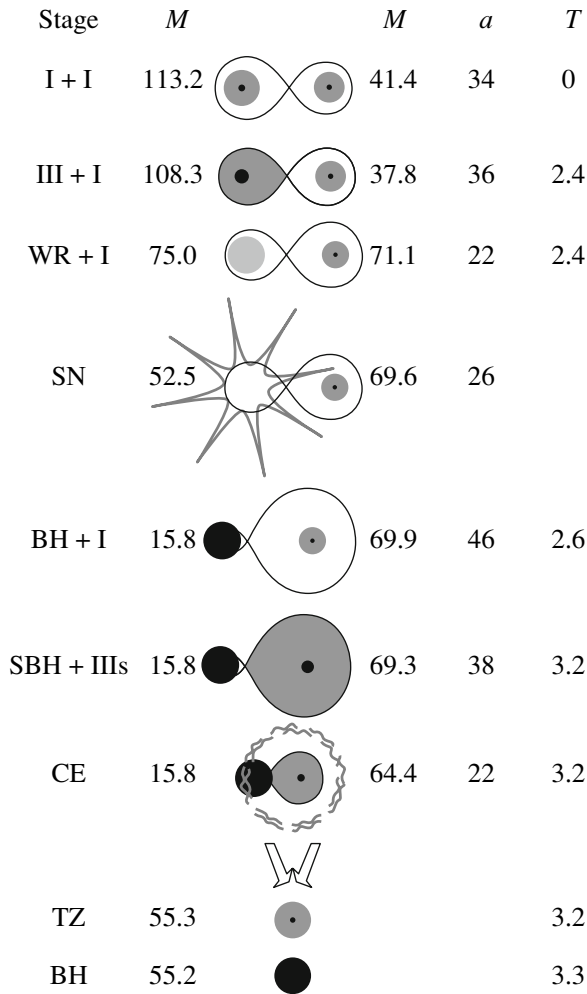
$$M_{BH} = k_{bh}M_{preSN}, \quad (2)$$

where the factor  $k_{bh}$  is the fraction of the mass of the pre-supernova enclosed by the event horizon during the collapse.

The factors  $\alpha$  and  $k_{WR}$  took the values 0.3 (the standard value used for calculations in scenario A) and 0.1. The weak wind roughly imitates the metallicity of X-7, which is smaller than the solar value [9]; the galaxy IC 10 is also poor in metals (see, for example, [26]).  $k_{bh}$  was varied from 0.1 to 1.0.

In the course of the population synthesis, we took the X-7 system to be a binary that contains a black hole with mass  $m_{BH} = 14\text{--}17 M_{\odot}$  and a main-sequence star at the end of its evolution with mass  $m_v = 65\text{--}75 M_{\odot}$ ; the orbital period of the system is  $P_{orb} \lesssim 5^d$ . The IC 10 X-1 system is represented in the calculations as a binary containing a black hole with mass  $m_{BH} = 23\text{--}34 M_{\odot}$  and a Wolf–Rayet star with mass  $m_{WR} = 17\text{--}35 M_{\odot}$ ; the orbital period is  $P_{orb} \lesssim 1.5^d$ . A population synthesis for  $10^6$  binaries was carried out for each set of parameters of the evolutionary scenario. The results suggest that X-7-type binaries should exist in galaxies with masses of at least  $10^{11} M_{\odot}$  and a star-formation rate specified by the Salpeter function. The number of such systems should currently be of the order of unity (Fig. 8). Figures 8–11 present the results for the calculations.

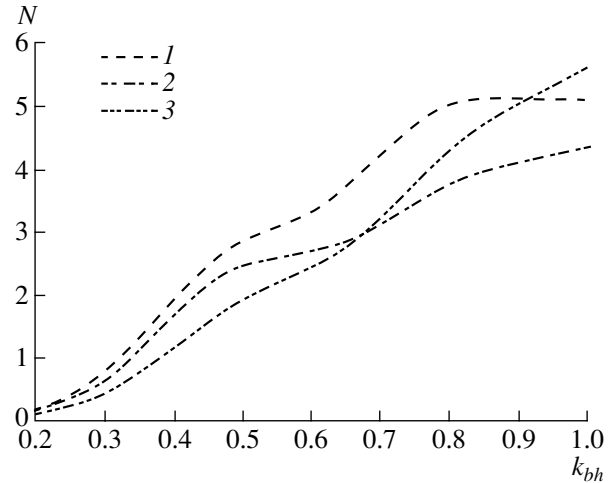
Figures 8 and 10 show the number of X-7-type and IC 10 X-1-type systems expected to occur in a spiral galaxy with a mass of  $10^{11} M_{\odot}$  and a star-formation rate specified by the Salpeter function. The numbers in the plots indicate curves calculated with (1)  $\alpha = 0.3$  and  $k_{WR} = 0.3$ , (2)  $\alpha = 0.1$  and  $k_{WR} = 0.1$ , and (3)  $\alpha = 0.1$  and  $k_{WR} = 0.3$ . Figure 8 shows that there exist values for  $k_{bh}$  for which X-7-type systems can be obtained. Taking into account that the star-formation rate, or at least the star-formation rate per square area, in M33 exceeds the average for spiral galaxies of the Local Group (see, for example, [27]), the existence of X-7 can be explained in scenario A. It is clear from Fig. 10 that IC 10 X-1-type systems can be obtained for a broad range of values of  $k_{bh}$ . Since the galaxy IC 10 has active star formation, we expect that the rate of formation of massive stars in IC 10



**Fig. 9.** A characteristic evolutionary scenario resulting in the formation of an M33 X-7-type system. The notation for the evolutionary stages is (see [23] for more detail): I — main-sequence stage, III, IIIs—stage of Roche-lobe filling, WR—Wolf–Rayet stage, BH—black hole, SBH—black hole with a supercritical accretion rate, SN—supernova explosion, CE—common-envelope stage, TZ—Thorne–Zhytkov object. The mass of the primary and secondary stars  $M$  (in  $M_{\odot}$ ), the semimajor axis  $a$  (in  $R_{\odot}$ ), and the age of the system  $T$  (in millions of years) are presented for the onsets of the corresponding stages and, in the case of the supernova explosion, for the time just before the explosion. The free parameters of the problem for this scenario are  $\alpha = 0.3$ ,  $k_{WR} = 0.3$ , and  $k_{bh} = 0.3$ .

is to order of magnitude comparable with this rate in the Milky Way (in spite of the fact that the mass of IC 10 is approximately two orders of magnitude lower than that of the Milky Way). A burst of star formation apparently started about 10 million years ago in IC 10 and is still ongoing (see, for example, [26, 28]).

Figure 9 presents a characteristic evolutionary scenario resulting in the formation of an X-7-type system. In all the scenarios in which such a sys-




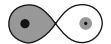

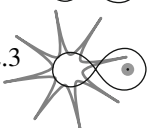



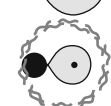

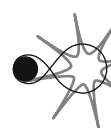




**Fig. 10.** Same as Fig. 8 for an IC 10 X-1-type system.

tem can be obtained, the qualitative scheme for the evolution of the binary is very similar. At the beginning of the evolution, this is a massive close binary, with a mass of the primary  $m_1 = 80\text{--}120 M_{\odot}$ , a mass of the secondary  $m_2 = 40\text{--}60 M_{\odot}$ , and an initial semimajor axis  $a \lesssim 100 R_{\odot}$ . The approximate intervals for the initial parameters of the precursors of X-7-type systems are also shown in Figs. 12 and 13. After the end of core hydrogen burning, the more massive primary fills its Roche lobe. Matter starts to flow to the secondary, as a rule, faster than on the nuclear timescale (stage III in [23]); the final part of the mass transfer can sometimes occur on close to this timescale (stage IIIe in [23]). When the primary has lost its envelope, it turns into a Wolf–Rayet star, which explodes and forms a black hole. The weak stellar wind in the main sequence stage, and also “correct selection” of the mass fraction of the pre-supernova that is enclosed by the event horizon during the formation of the black hole, make it possible to form a black hole of the required mass (around  $15\text{--}20 M_{\odot}$ ) in a sufficiently close system. Note also that an X-7-type system does not undergo a common-envelope stage before its formation.<sup>2</sup> Qualitatively, the subsequent evolution of an X-7-type binary is as follows. The secondary (initially less massive) star fills its Roche lobe, leading to a stage of supercritical accretion onto the black hole; a common-envelope then forms, and the binary ends

<sup>2</sup> See [23] for more detail. The “Scenario Machine” assumes that type B systems, according to the classification of Kippenhahn and Weigert [25], form a common envelope if  $q \leq q_{cr} = 0.3$ . Here,  $q = M_{accretor}/M_{donor}$  is the ratio of the masses of the primary (accretor) and secondary (donor) stars. For the track presented in Fig. 9,  $q \approx 0.35$  at the beginning of the stage of Roche-lobe filling of the initially more massive primary star.



Stage	$M$		$M$	$a$	$T$
I + I	94.3		56.7	180	0
III + I	92.5		56.2	190	2.5
IIIe + I	60.8		60.8	180	2.5
WR + I	58.1		61.0	180	3.1
SN	52.3		61.0	190	
BH + I	26.1		61.0	270	3.3
BH + II	26.1		60.9	270	3.5
SBH + IIIs	26.1		54.5	270	3.8
CE	26.1		53.0	260	3.8
BH + WR	26.1		31.6	18	3.8
SN	26.1		28.4	19	
BH + BH	26.1		14.2	30	4.1
BH	40.3				4300

**Fig. 11.** A characteristic evolutionary scenario resulting in the formation of an IC 10 X-1-type system. The notation for the evolutionary stages is (see [23] ] for more detail): I—main-sequence star; II—star has ended its evolution on the main sequence but does not fill its Roche lobe; III, IIIe, and IIIs—stage of Roche-lobe filling; WR—Wolf–Rayet stage; BH—black hole; SBH—black hole with a supercritical accretion rate; SN—supernova explosion; CE—common-envelope stage. The mass of the primary and secondary stars  $M$  (in  $M_{\odot}$ ), the semimajor axis  $a$  (in  $R_{\odot}$ ), and the age of the system  $T$  (in millions of years) are presented for the onsets of the corresponding stages and, in the case of the supernova explosion, for the time just before the explosion. The free parameters of the problem in this scenario are  $\alpha = 0.1$ ,  $k_{WR} = 0.1$ ,  $k_{bh} = 0.5$ .

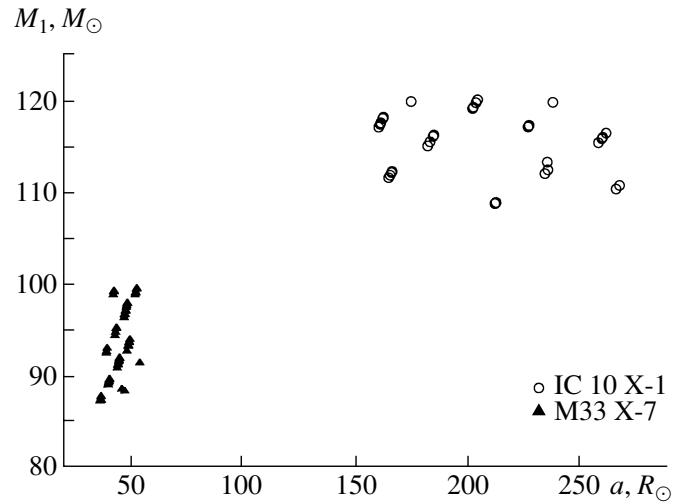
its existence with the merger of its components and the formation of a Thorne–Zhytkov object. The final result of the evolution of an X-7-type system is a single massive black hole. When the black hole moves along a spiral trajectory into the center of the non-degenerate star (the Thorne–Zhytkov object stage), the system can be a source of gravitational waves [29].

Let us now consider the characteristic evolutionary track of a binary that results in the formation

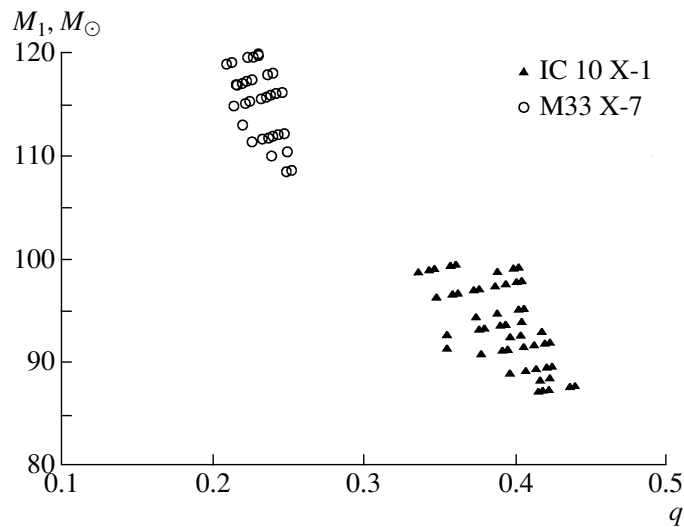
of an IC 10 X-1-type system (Fig. 11). At the beginning of the evolution, the mass of the primary is  $m_1 = 80\text{--}120 M_{\odot}$ , the mass of the secondary is  $m_2 = 15\text{--}60 M_{\odot}$ , and the initial semimajor axis of the binary orbit is  $a \simeq 170\text{--}200 R_{\odot}$ . The approximate intervals of the initial parameters of precursors of IC 10 X-1-type systems are also shown in Figs. 12 and 13. Note that, since the mass of a star can exceed its initial mass due to mass transfer, the minimum initial mass of the secondary can be lower than the estimated mass for the Wolf–Rayet star in IC 10 X-1. After the depletion of hydrogen in its core, the more massive primary fills its Roche lobe. Matter starts to flow to the secondary, as a rule, faster than on the nuclear timescale (stage III in [23]); the final part of the mass transfer occurs on a timescale close to the nuclear timescale (stage IIIe in [23]). When the primary has lost its envelope, it turns into a Wolf–Rayet star, which explodes and forms a black hole. Further, the secondary finishes its evolution on the main sequence and fills its Roche lobe. After a phase of supercritical accretion onto the black hole during the Roche-lobe filling stage, a common-envelope stage begins, during which the stars approach each other very closely and the non-relativistic component loses its envelope. A binary consisting of a black hole and a Wolf–Rayet star is formed. In the process of collapse of the Wolf–Rayet star the gamma-burst may occur in such a binary. The evolution of an IC 10 X-1-type binary ends with the merging of the two black holes (remnants of the evolution of the system components), driven by gravitational-wave radiation, resulting in the formation of a single massive black hole. The merger should be accompanied by a burst of gravitational-wave radiation.

## 5. CONCLUSION

We have used the radial-velocity curve for the optical star in the M33 X-7 system [9] and parameters of the system derived from an analysis of the light curve [9] ( $\mu = 0.78$ ,  $i = 74^{\circ}.6$ ) to construct the relationship between the masses of the black hole  $m_x$  and the optical star  $m_v$  (Table 2, Fig. 6) in a Roche model for the optical star. We also studied the effect of tidal deformation and gravitational darkening of the optical star on the mass of the black hole  $m_x$  for various degrees of filling of the Roche lobe of the optical star  $\mu$  (Table 3). For  $\mu = 0.78$ , the impact of the proximity of the components on the radial-velocity curve of the optical star is relatively small, justifying the analysis used by Orosz et al. [9] to derive the black-hole mass  $m_x = 15.65 \pm 1.45 M_{\odot}$  (for  $m_v = 70 M_{\odot}$ ). Our estimated mass for the black hole for  $m_v = 70 M_{\odot}$  coincides with this value within the errors:  $m_x = 15.55 \pm 3.20 M_{\odot}$ ; the error corresponds to the 95%



**Fig. 12.** Initial parameters of systems that evolve into binaries of the type considered. The vertical axis plots the initial mass of the primary (which is initially more massive) and the horizontal axis the initial semimajor axis of the system. The triangles and circles indicate binaries that evolve to form M33 X-7-type and IC 10 X-1-type systems, respectively. The free parameters of the problem in this case are  $\alpha = 0.1$ ,  $k_{WR} = 0.1$ ,  $k_{bh} = 0.3$ .



**Fig. 13.** Initial parameters of systems that evolve into binaries of the type considered. The vertical axis plots the initial mass of the primary (which is initially more massive) and the horizontal axis the component-mass ratio  $q = M_2/M_1 < 1$  at the beginning of the system's evolution. The notation is the same as in Fig. 12. The free parameters of the problem in this case are  $\alpha = 0.1$ ,  $k_{WR} = 0.1$ ,  $k_{bh} = 0.3$ .

confidence interval for  $\chi_M^2$  statistics, where  $M$  is the number of data points in the radial-velocity curve. We stress that, if the degree of Roche-lobe filling by the optical star  $\mu$  were close to unity, with all other factors being the same, the black-hole mass would be  $m_x = 15.95 \pm 3.2 M_\odot$ , which exceeds the value for  $\mu = 0.78$  by  $\sim 3\%$ . Therefore, it is important to use a more realistic Roche model that takes into account the tidal-rotational deformation of the optical star and its gravitational darkening, rather than a point-mass model, when fitting the radial-velocity curve.

We also considered the evolutionary status of the

X-ray binaries M33 X-7 and IC 10 X-1, and have shown that the existence of such systems, which probably contain massive stellar black holes, is quite possible in the galaxies M33 and IC 10 for reasonable physical assumptions about the initial parameters of these systems and the mass transfer in them. In the evolution process the IC 10X-1 system should pass through the stage, during which it will consist of a black hole and the Wolf-Rayet star. At the instant of collapse of the Wolf-Rayet star the gamma-burst may occur in this binary. We conclude that the evolution of the IC 10 X-1 system should end with a

merger of two massive black holes, which should result in a burst of gravitational-wave radiation. In the case of the X-7 system, a burst of gravitational wave radiation should be observed during the formation of a Thorne–Zhytkov object [29]. These conclusions are important for observational programs to be undertaken with modern laser gravitational-wave telescopes, such as LIGO, VIRGO, etc.

Note that the detection of a black hole in M33 X-7 [9] has opened the era of searches for black holes in other galaxies of the Local Group. This has become possible due to the commissioning of large, 8–10-m, new-generation telescopes. The first detections of new stellar-mass black holes in other galaxies are consistent with the hypothesis that there is a bimodal mass distribution for relativistic objects [30–32]. This distribution and the presence of a dip in the mass distribution for neutron stars and black holes in the range  $m_x = 2-4 M_\odot$  [30] were first deduced from the masses of about 40 objects ( $\sim 20$  neutron stars and  $\sim 20$  black holes). The detection of new black holes in other galaxies will make it possible to substantially increase the number of mass estimates for relativistic objects, and thus to improve the significance of corresponding statistical conclusions. The increase in the number of detected black holes in X-ray binaries will also open fresh opportunities for verifying new theories of gravitation [32, 33].

#### ACKNOWLEDGMENTS

The authors thank V.V. Shimanskii for his assistance in the calculations and useful discussions, as well as A.V. Tutukov for valuable comments. The work was supported by the Russian Foundation for Basic Research (project code 08-02-01220), the State Program of Support for Leading Scientific Schools of the Russian Federation (grant NSh-1685.2008.2), a Presidential Grant of the Russian Federation to Support Young Russian Candidates of Science (MK-2059.2007.2), and the Analytical Departmental Targeted Program “The Development of Higher Education Science Potential” (grant RNP-2.1.1.5940).

#### REFERENCES

1. K. S. Long, S. Dodorico, P. A. Charles, and M. A. Dopita, *Astrophys. J.* **246**, L61 (1981).
2. G. Peres, F. Reale, A. Collura, and G. Fabbiano, *Mem. Soc. Astron. Ital.* **60**, 221 (1989).
3. G. Peres, F. Reale, A. Collura, and G. Fabbiano, *Astrophys. J.* **336**, 140 (1989).
4. D. T. Larson and E. Schulman, *Astron. J.* **113**, 618 (1997).
5. G. Dubus, P. A. Charles, K. S. Long, et al., *Mon. Not. R. Astron. Soc.* **302**, 731 (1999).
6. W. Pietsch, F. Haberl, M. Sasaki, et al., *Astrophys. J.* **646**, 420 (2006).
7. W. Pietsch, B. J. Mochejska, Z. Misanovic, et al., *Astron. Astrophys.* **413**, 879 (2004).
8. A. Shporer, J. Hartman, T. Mazeh, and W. Pietsch, *Astron. Astrophys.* **462**, 1091 (2007).
9. J. A. Orosz, J. E. McClintock, R. Narayan, et al., *Nature* **449**, 872 (2007).
10. E. A. Antokhina and A. M. Cherepashchuk, *Astron. Zh.* **71**, 420 (1994) [*Astron. Rep.* **38**, 367 (1994)].
11. E. A. Antokhina, *Astron. Zh.* **73**, 532 (1996) [*Astron. Rep.* **40**, 483 (1996)].
12. R. L. Kurucz, *Kurucz CD-Roms* (Smithsonian Astrophys. Observ., Cambridge, MA, USA, 1993).
13. J. Diaz-Cordoves and A. Gimenez, *Astron. Astrophys.* **227**, 259 (1992).
14. W. Van Hamme, *Astron. J.* **106**, 2096 (1995).
15. A. M. Cherepashchuk, *Astron. Zh.* **70**, 1157 (1993) [*Astron. Rep.* **37**, 585 (1993)].
16. E. A. Antokhina, A. M. Cherepashchuk, and V. V. Shimanskii, *Astron. Zh.* **82**, 131 (2005) [*Astron. Rep.* **49**, 109 (2005)].
17. M. K. Abubekero, *Astron. Zh.* **81**, 714 (2004) [*Astron. Rep.* **48**, 649 (2004)].
18. M. K. Abubekero, E. A. Antokhina, and A. M. Cherepashchuk, *Astron. Zh.* **81**, 108 (2004) [*Astron. Rep.* **48**, 89 (2004)].
19. M. K. Abubekero, E. A. Antokhina, and A. M. Cherepashchuk, *Astron. Zh.* **81**, 606 (2004) [*Astron. Rep.* **48**, 550 (2004)].
20. M. K. Abubekero, E. A. Antokhina, A. M. Cherepashchuk, and V. V. Shimanskii, *Astron. Zh.* **83**, 609 (2006) [*Astron. Rep.* **50**, 544 (2006)].
21. J. M. Silverman and A. V. Filippenko, arXiv:0802.2716v [astro-ph] (2008).
22. V. M. Lipunov, K. A. Postnov, and M. E. Prokhorov, *Astrophys. Space Phys. Rev.* **9**, 1 (1996).
23. V. M. Lipunov, K. A. Postnov, M. E. Prokhorov, et al., arXiv:0704.1387v2 [astro-ph] (2007).
24. A. I. Bogomazov, M. K. Abubekero, and V. M. Lipunov, *Astron. Zh.* **82**, 722 (2005) [*Astron. Rep.* **49**, 644 (2005)].
25. R. Kippenhahn and A. Weigert, *Z. Astrophys.* **65**, 251 (1967).
26. P. Massey, K. A. G. Olsen, P. W. Hodge, et al., *Astron. J.* **133**, 2393 (2007).
27. E. Gardan, J. Braine, K. F. Schuster, et al., *Astron. Astrophys.* **473**, 91 (2007).
28. W. D. Vacca, C. D. Sheehy, and J. R. Graham, *Astrophys. J.* **662**, 272 (2007).
29. S. N. Nazin and K. A. Postnov, *Astron. Astrophys.* **303**, 789 (1995).
30. A. M. Cherepashchuk, *Astron. Zh.* **78**, 145 (2001) [*Astron. Rep.* **45**, 120 (2001)].
31. A. M. Cherepashchuk, *Usp. Fiz. Nauk* **173**, 345 (2003) [*Phys. Usp.* **46**, 139 (2003)].
32. K. A. Postnov and A. M. Cherepashchuk, *Astron. Zh.* **80**, 1075 (2003) [*Astron. Rep.* **47**, 989 (2003)].
33. T. Johannsen, D. Psaltis, and J. E. McClintock, e-Print arXiv:08031835v1 [astro-ph] (2008).

*Translated by K. Maslennikov*